

NASA TM-100884

NASA Technical Memorandum 100884

NASA-TM-100884 19880016551

Improved Method for Stress and Compatibility Analysis of Multi-component Rotating Systems

Gerald A. Carek
Lewis Research Center
Cleveland, Ohio

June 1988

LIBRARY USE

AUG 26 1988

LANGLEY RESEARCH CENTER
LIBRARY NASA
HAMPTON, VIRGINIA

NASA

IMPROVED METHOD FOR STRESS AND COMPATIBILITY ANALYSIS OF
MULTICOMPONENT ROTATING SYSTEMS

Gerald A. Carek
National Aeronautics and Space Administration
Lewis Research Center
Cleveland, Ohio 44135

SUMMARY

An improved method of analyzing multicomponent rotating assemblies for the determination of operating stresses and component compatibility has been developed. In this method, a single finite element model is developed which contains all of the separate components in the rotating assembly. This is made possible by using gap elements to simulate the contact surfaces between components. The MARC finite element computer program is then used to perform the analysis.

This improved method is less time consuming and more reliable than the conventional method of analyzing such systems. Previously, a method called the flexibility method was used at the NASA Lewis Research Center for this task. It requires the individual analysis of components, derivation of compatibility equations, determination of certain coefficients for these equations, and an iterative solution procedure.

This report presents results for two different stress-compatibility analyses of a six-component axial flow compressor rotor. The results for the flexibility analysis method are compared with those for the improved analysis method. It was found that the stresses predicted by each method compare quite well with each other. The predictions of the component compatibility, as well as the magnitude of the forces at the contact surfaces, also compare well for these two analysis procedures. It is therefore recommended that the improved analysis method be used to determine the stress-compatibility characteristics of multicomponent rotating systems.

INTRODUCTION

Much of the rotating hardware in turbomachinery - such as the rotors of compressors, turbines, pumps, and blowers - is designed as an assembly of several components which are mated together by means of an external-internal pilot interface. A typical pilot design is shown in figure 1. A tight pilot interface is essential in rotating machinery since it maintains the concentricity of separate components that are rotating about the same axis. In some cases the engineer may take advantage of the supporting characteristics of the pilot interface - the outer (enclosing) part provides radial support to the inner part. However, as an assembly of components is subjected to certain loading conditions, such as centrifugal loading, one of the outer parts may expand (in the radial direction) more than its adjacent inner part. This can loosen the parts and upset the integrity of the assembly. One of the difficulties in designing a pilot feature is that the pilot surfaces must be orientated such that the inner part expands at a greater rate than the outer part. In some

N88-25935 #

cases, a sufficient assembly interference fit can be chosen that ensures that the parts will not separate when subjected to centrifugal loads.

The rotating assembly of parts is usually held together by axial pre-loaded bolts or rods. Multiple tie bolts are sometimes used in a circular pattern. A single tie bolt, which lies along the rotational axis of the machine, can also be used.

Rotating hardware that is designed in such a manner is subjected to several loading conditions while in operation. These conditions include centrifugal forces due to rotation, axial forces due to the preloaded bolts or rods, and pilot surface forces due to initial pilot interference fits. Other loading may include forces caused by transient or steady-state thermal distribution, pressure forces, or aerodynamic forces.

To properly determine the stresses and deflections of this type of assembly, the analyst cannot simply analyze each component independently and insure that the pilot interfaces are designed in the proper external-internal orientation. The forces at each contacting surface are dependent on the forces at any or all of the other contacting surfaces within the assembly. For example, the increasing pressure at one pilot interface (due to centrifugal loading) may cause the pressure at an adjacent pilot interface to decrease, possibly forming a gap between two parts. Another consideration is that the pilot pressures, as well as the axial clamping force due to the tie bolt preload, contribute to the stress distribution on the assembly.

The design and analysis are complicated further because several considerations must be taken into account when selecting the tie bolt preload. For instance, as an assembly of rotating parts increase in speed, the Poisson's ratio effect tends to shrink the axial dimensions of the assembly, thus reducing the load on the bolt holding the components together. If the preload in the bolt diminishes to zero, the parts will loosen, causing an unbalance and possibly catastrophic results. Therefore it is very important to be able to accurately determine what preload remains in the bolt at operating conditions.

The conventional method of analysis that has been used at NASA Lewis for this type of assembly is based on the use of the principle of complementary energy. This conventional method requires that each component of the rotating assembly be analyzed separately (usually a finite element analysis) under a variety of loading conditions in order to determine the interdependence of the contacting surfaces, such as the displacement of one surface due to a load at another surface. These interdependencies are described as influence coefficients, and are determined for each component in the assembly. An equilibrium equation is then derived for every contacting point in the assembly, by equating the displacements of the two surfaces in contact. These equations contain the previously determined influence coefficients, displacement at the contact surfaces due to operating loads, interference fits of the pilots, and pressure forces at the interface of the contact points. The interface pressure forces are the unknowns in each equation and must be determined by solving a system of N equations and N unknowns where N is the number of contacting points in the assembly. Once the system of equations is solved, the analyst can determine if contacting surfaces remain closed. If gaps develop, or if the tie bolt cannot hold the assembly of components together at operating conditions, then design modifications must be made and the analysis repeated. Aside

from being very time consuming, this type of analysis involves the manipulation of large quantities of numbers and is very prone to mistakes. Errors are not obvious and may go unnoticed throughout the analysis, giving false results.

Other methods for analyzing this type of assembly exist (ref. 1), and they usually utilize the principle of minimum total potential energy. For all of the methods, a set of equilibrium equations must be solved to determine the unknown forces of a statically indeterminate structure.

An improved method of analyzing multicomponent rotating systems has been developed which utilizes the MARC finite element computer program. By using MARC gap elements to simulate the points of contact, the entire assembly of components can be represented in a single finite element model. Therefore it is not required to develop and solve a system of equilibrium equations, nor to analyze each component separately for the determination of influence coefficients. Also, any changes that must be made in the design are simply done by modifying the model that represents the complete assembly. This method significantly reduces the time and effort required for such an analysis.

The objective of this report is to describe the improved method of analysis. A stress-compatibility analysis of a seven-component axial flow compressor rotor has been performed, using the two methods described above, and the results are compared.

SYMBOLS

du	incremental displacement vector
df	incremental force vector
K	stiffness matrix
k_{ij}	displacement at point i in the direction of P_j due to a load P_j (influence coefficients)
N	number of contacting points in the assembly
P_B	force due to the tie bolt
P_i	contact force at interface i (integrated around the circumference)
P_1, P_3, P_5, P_7, P_9	radial pressure forces corresponding to the pilot interfaces
P_2, P_4, P_6, P_8	forces that tend to rotate the radial contact surfaces between components
S_1	shrink (in axial direction) of all rotor components, due to radial pilot forces and compression from the tie bolt
S_2	shrink (in axial direction over the length of the tie bolt) of all rotor components, due to centrifugal and thermal loading

S3	shrink (in axial direction) of the tie bolt, due to centrifugal and thermal loading
ΔB	stretch of the tie bolt caused by the axial force, P_B , in the tie bolt
ΔL	total initial axial stretch in the tie bolt that would be required to cause the axial forces, P_B , to be just equal to zero
Δy_i	initial pilot interference fit in the direction of P_i
δ_i	displacement at point i in the direction of P_i due to centrifugal and thermal loading only ¹

Superscripts:

D1,D2,D3,D4	disks 1, 2, 3, 4
FS	front shaft
RS	rear shaft
TB	tie bolt

Subscripts:

i,j	designations for i and j are 1 to 9 and B
-----	---

DESCRIPTION OF COMPRESSOR

The compressor rotor that was analyzed is from the three-stage axial flow compressor shown in figure 2. This is an aerodynamic research compressor which is driven by a variable-speed electric motor through a speed increasing gearbox. The rotor design includes a single tie bolt and is composed of six separate components: a front shaft, four disks, and a rear shaft (fig. 3). Compressor blades are integrally machined into the first three disks, and the fourth disk is used as an axial spacer. The blades were not included in this analysis, but were left for a separate detailed analysis, although the centrifugal forces caused by them were considered.

The four disks are mated together by means of a external-internal pilot interface, and the pilot diameters are dimensioned such that there is a 0.0254-mm (0.001-in.) radial interference fit between the mating parts. The disks are axially bolted to the rear shaft by a single tie bolt which lies along the axis of rotation. During assembly, the tie bolt must be torqued such that its preload will prevent gaps from forming at the axial contact surfaces between mating parts. After the tie bolt is installed, the front

¹Displacements due to forces P_2 , P_4 , P_6 , and P_8 are taken to be the differences in the axial displacements at the outer and inner points where the forces are applied.

shaft is mated to the first disk by means of a pilot, and it is axially bolted with four bolts located on a 63.5 mm (2.5 in.) diameter.

The compressor components are constructed of the following materials: titanium alloy Ti-6Al-4V for the four disks, AISI 4340 alloy steel for the front and rear shafts, and 18 percent nickel alloy maraging steel (200 ksi) for the tie bolt. The material properties that were used in the analysis are shown in table I.

The compressor rotor was analyzed at an operating speed of 47 500 rpm. The airflow through the compressor varied in temperature from 15 °C (60 °F) at the inlet to 182 °C (360 °F) after the third stage of compressor blades. The operating temperature for the bearings was 82 °C (180 °F).

FLEXIBILITY ANALYSIS METHOD

This particular analysis technique is sometimes referred to as the flexibility method and is based on the principle of complementary energy. References 2 to 4 describe the theoretical background pertaining to the principle of complementary energy, and a general description for the applications of this method is given in references 5 and 6. The analysis involves the formulation and solution of a set of equilibrium equations hereafter referred to as compatibility equations. The general equations are derived using the principle of superposition in which the deflections of any two components, due to all applied known and unknown loading, are equated at their interface. One equation is derived for each contacting surface in the assembly of components that make up the compressor rotor. The satisfaction of these equations indicates that the surfaces are compatible and that no gaps develop between parts. The equations are written in matrix form, and a simultaneous solution must be performed to solve for the unknown forces. The solution may indicate impossible loads, such as a tensile force across a contacting surface. In this case, the tensile forces must be set equal to zero, and another solution must be obtained. This iterative process is complicated by the fact that there is an interdependence of the effects of the unknown forces.

The FEATS finite element computer program (ref. 7) was used to analyze the seven components of the compressor rotor separately in order to determine the values of certain coefficients contained within the set of compatibility equations. Two-dimensional four-noded quadrilateral axisymmetric elements were used in the modeling. The finite element models, along with the unknown interacting forces, are shown in figure 4. Since there are 10 unknown forces on the assembly, the compatibility equations will be described with a 10 by 10 matrix. The forces P_1 , P_3 , P_5 , P_7 , and P_9 are radial pressure forces corresponding to the pilot interfaces. Forces that tend to rotate the radial contact surfaces between components are described as P_2 , P_4 , P_6 , and P_8 . Notice that these forces only create a moment on the surfaces. The force that is imposed on the components due to the tie bolt is P_B .

By equating the displacements at each of the contacting surfaces (1 to 9), the following compatibility equations were derived:

Surface 1:

$$K_{11}^{FS}P_1 + \delta_1^{FS} = K_{11}^{D1}P_1 + K_{12}^{D1}P_2 + K_{13}^{D1}P_3 + K_{1B}^{D1}P_B + \delta_1^{D1} + \Delta y_1 \quad (1)$$

Surface 2:

$$\begin{aligned} K_{21}^{D1} p_1 + K_{22}^{D1} p_2 + K_{23}^{D1} p_3 + K_{2B}^{D1} p_B + \delta_2^{D1} = \\ K_{22}^{D2} p_2 + K_{23}^{D2} p_3 + K_{24}^{D2} p_4 + K_{25}^{D2} p_5 + K_{2B}^{D2} p_B + \delta_2^{D2} \end{aligned} \quad (2)$$

Surface 3:

$$\begin{aligned} K_{31}^{D1} p_1 + K_{32}^{D1} p_2 + K_{33}^{D1} p_3 + K_{3B}^{D1} p_B + \delta_3^{D1} = \\ K_{32}^{D2} p_2 + K_{33}^{D2} p_3 + K_{34}^{D2} p_4 + K_{35}^{D2} p_5 + K_{3B}^{D2} p_B + \delta_3^{D2} + \Delta y_3 \end{aligned} \quad (3)$$

Surface 4:

$$\begin{aligned} K_{42}^{D2} p_2 + K_{43}^{D2} p_3 + K_{44}^{D2} p_4 + K_{45}^{D2} p_5 + K_{4B}^{D2} p_B + \delta_4^{D2} = \\ K_{44}^{D3} p_4 + K_{45}^{D3} p_5 + K_{46}^{D3} p_6 + K_{47}^{D3} p_7 + K_{4B}^{D3} p_B + \delta_4^{D3} \end{aligned} \quad (4)$$

Surface 5:

$$\begin{aligned} K_{52}^{D2} p_2 + K_{53}^{D2} p_3 + K_{54}^{D2} p_4 + K_{56}^{D2} p_6 + K_{5B}^{D2} p_B + \delta_5^{D2} = \\ K_{54}^{D3} p_4 + K_{55}^{D3} p_5 + K_{56}^{D3} p_6 + K_{57}^{D3} p_7 + K_{5B}^{D3} p_B + \delta_5^{D3} + \Delta y_5 \end{aligned} \quad (5)$$

Surface 6:

$$\begin{aligned} K_{64}^{D3} p_4 + K_{65}^{D3} p_5 + K_{66}^{D3} p_6 + K_{67}^{D3} p_7 + K_{6B}^{D3} p_B + \delta_6^{D3} = \\ K_{66}^{D4} p_6 + K_{67}^{D4} p_7 + K_{68}^{D4} p_8 + K_{69}^{D4} p_9 + K_{6B}^{D4} p_B + \delta_6^{D4} \end{aligned} \quad (6)$$

Surface 7:

$$\begin{aligned} K_{74}^{D3} p_4 + K_{75}^{D3} p_5 + K_{76}^{D3} p_6 + K_{77}^{D3} p_7 + K_{7B}^{D3} p_B + \delta_7^{D3} = \\ K_{76}^{D4} p_6 + K_{77}^{D4} p_7 + K_{78}^{D4} p_8 + K_{79}^{D4} p_9 + K_{7B}^{D4} p_B + \delta_7^{D4} + \Delta y_7 \end{aligned} \quad (7)$$

Surface 8:

$$\begin{aligned} K_{86}^{D4} p_6 + K_{87}^{D4} p_7 + K_{88}^{D4} p_8 + K_{89}^{D4} p_9 + K_{8B}^{D4} p_B + \delta_8^{D4} = \\ K_{88}^{RS} p_8 + K_{89}^{RS} p_9 + K_{8B}^{RS} p_B + \delta_8^{RS} \end{aligned} \quad (8)$$

Surface 9:

$$K_{96}^{D4}P_6 + K_{97}^{D4}P_7 + K_{98}^{D4}P_8 + K_{99}^{D4}P_9 + K_{9B}^{D4}P_B + \delta_9^{D4} = \\ K_{98}^{RS}P_8 + K_{99}^{RS}P_9 + K_{9B}^{RS}P_B + \delta_9^{RS} + \Delta y_9 \quad (9)$$

The compatibility equation for the contact surface located at the head of the tie bolt was derived as follows:

$$\Delta B = \Delta L - S1 - S2 + S3 \quad (10)$$

where

$$S1 = K_{B1}^{D1}P_1 + K_{B2}^{D1}P_2 + K_{B3}^{D1}P_3 + K_{BB}^{D1}P_B \\ + K_{B2}^{D2}P_2 + K_{B3}^{D2}P_3 + K_{B4}^{D2}P_4 + K_{B5}^{D2}P_5 + K_{BB}^{D2}P_B \\ + K_{B4}^{D3}P_4 + K_{B5}^{D3}P_5 + K_{B6}^{D3}P_6 + K_{B7}^{D3}P_7 + K_{BB}^{D3}P_B \\ + K_{B6}^{D4}P_6 + K_{B7}^{D4}P_7 + K_{B8}^{D4}P_8 + K_{B9}^{D4}P_9 + K_{BB}^{D4}P_B \\ + K_{B8}^{RS}P_8 + K_{B9}^{RS}P_9 + K_{BB}^{RS}P_B \quad (11)$$

$$S2 = \delta_B^{D1} + \delta_B^{D2} + \delta_B^{D3} + \delta_B^{D4} + \delta_B^{RS} \quad (12)$$

$$S3 = \delta_B^{TB} \quad (13)$$

$$\Delta B = K_{BB}^{TB}P_B \quad (14)$$

Rearranging equation (11) gives

$$S1 = K_{B1}^{D1}P_1 + \left(K_{B2}^{D1} + K_{B2}^{D2} \right)P_2 + \left(K_{B3}^{D1} + K_{B3}^{D2} \right)P_3 \\ + \left(K_{B4}^{D2} + K_{B4}^{D3} \right)P_4 + \left(K_{B5}^{D2} + K_{B5}^{D3} \right)P_5 + \left(K_{B6}^{D3} + K_{B6}^{D4} \right)P_6 \\ + \left(K_{B7}^{D3} + K_{B7}^{D4} \right)P_7 + \left(K_{B8}^{D4} + K_{B8}^{RS} \right)P_8 + \left(K_{B9}^{D4} + K_{B9}^{RS} \right)P_9 \\ + \left(K_{BB}^{D1} + K_{BB}^{D2} + K_{BB}^{D3} + K_{BB}^{D4} + K_{BB}^{RS} \right)P_B \quad (15)$$

and equation (10) is rewritten as

$$S1 + \Delta B = \Delta L - S2 + S3 \quad (16)$$

and substitution of equations (12) to (15) into equation (16) yields the 10th compatibility equation which is

$$\begin{aligned} K_{B1}^{D1} P_1 + \left(K_{B2}^{D1} + K_{B2}^{D2} \right) P_2 + \left(K_{B3}^{D1} + K_{B3}^{D2} \right) P_3 + \left(K_{B4}^{D2} + K_{B4}^{D3} \right) P_4 \\ + \left(K_{B5}^{D2} + K_{B5}^{D3} \right) P_5 + \left(K_{B6}^{D3} + K_{B6}^{D4} \right) P_6 + \left(K_{B7}^{D3} + K_{B7}^{D4} \right) P_7 \\ + \left(K_{B8}^{D4} + K_{B8}^{RS} \right) P_8 + \left(K_{B9}^{D4} + K_{B9}^{RS} \right) P_9 + \left(K_{BB}^{D1} + K_{BB}^{D2} + K_{BB}^{D3} + K_{BB}^{D4} + K_{BB}^{RS} \right) P_B \\ + K_{BB}^{TB} P_B = \Delta L - \left(\delta_B^{D1} + \delta_B^{D2} + \delta_B^{D3} + \delta_B^{D4} + \delta_B^{RS} \right) + \delta_B^{TB} \end{aligned} \quad (17)$$

Each of the components that make up the compressor rotor assembly were separately analyzed with the FEATS program in order to determine the k_{ij} and the δ_j terms in the compatibility equations. The components were first analyzed under centrifugal and thermal loading conditions only (effects of the forces, P_i , were neglected) in order to determine the δ_j terms. The blade loads were applied as distributed nodal point loads and the temperature distribution over the components was manually input by prescribing a temperature for each element. These elemental temperatures were obtained from a previous steady-state heat transfer analysis. The δ_j terms for the compatibility equations were then determined by noting the resulting nodal displacements at the contacting surface(s) of each component. This procedure required a total of seven separate computer runs. Next, the k_{ij} terms (influence coefficients) were determined by loading each component with a trial load at a contact surface (j) and noting the resulting nodal displacement at some contact surface (i). No other loads were applied to the component. Several trial load conditions had to be applied to each component in order to obtain all of the influence coefficients. This was the most time-consuming portion of the analysis since it required 24 separate computer runs to determine the 102 influence coefficients.

Since the pilot interfaces in the assembly are designed with a 0.0254-mm (0.001-in.) radial interference fit, the Δy_j terms in the compatibility equations were set to 0.0254 mm (0.001 in.). Notice that this is a differential deflection term which can be placed on either side of the equation according to a chosen sign convention.

The desired tie bolt preload was chosen to be 47 148 N (10 600 lb). For the given bolt size, this load results in a bolt elongation of approximately 0.508 mm (0.020 in.). Therefore the ΔL term in the 10th compatibility equation (eq. (10)) was set to 0.508 mm (0.020 in.).

Once the general formation of the 10 compatibility equations was accomplished, the equations were rearranged in matrix form by transforming unknown terms, P_i , and their coefficients to the left side, and the known terms to the

right side. An initial solution of the set of equations yielded negative values for some of the axial forces; therefore those forces were set equal to zero and another solution was obtained. After several iterations, it was found that the forces P_2 , P_4 , P_6 , and P_8 were all equal to zero. The values of the forces in the radial direction all turned out to be positive, which indicates that no gaps will develop at the pilot interfaces during operation. Also, the load P_B was positive, which means that the tie bolt remains loaded during operation.

After the interacting forces on the assembly were determined, another individual finite element analysis of the components was performed, including these forces, to determine the final operating stresses of the compressor rotor.

IMPROVED ANALYSIS METHOD

For this analysis technique, a two-dimensional finite element model of the entire compressor was developed which incorporates all of the components and also properly simulates the effects of all contacting surfaces. The analysis, which uses the MARC finite element computer program (ref. 8), was done in two parts. The first part was a heat transfer analysis that determined the steady-state temperature distribution over the compressor due to the airstream temperatures and bearing operating temperatures. The resulting elemental temperatures were saved on a computer tape and later incorporated into the computer analysis that was performed for the stress-compatibility analysis.

The finite element mesh shown in figure 5 is comprised of 371 eight-node quadrilateral axisymmetric elements. The mesh actually consists of six separate finite element models joined together by MARC gap elements; the gap elements were placed at the surfaces that are in contact. There are 10 contacting surfaces in the model, 5 are the pilot interfaces, and 5 are the surfaces that are held tightly together by the force of the tie bolt. These 10 surfaces were modeled with 20 fixed-direction gap elements, 2 gap elements per surface. Ten of the gap elements were orientated in the radial direction and model the pilot contact surfaces, while the other 10 were orientated in the axial direction and model the surfaces that are held together by the tie bolt. Note that the tie bolt was integrated within the rear shaft since the assumption was made that the threaded connection of the tie bolt is rigid.

The gap elements can be defined with either a closure distance or an interference fit. If a closure distance is chosen, the contacting surfaces are initially assumed to be separated by that distance (i.e., a gap exists). On the other hand, if an interference fit is chosen, the surfaces are initially assumed to be in contact. In this case, the MARC program simulates the pressure loading on the surfaces by forcing the two end nodes of the gap element (there is one node on each surface) to be displaced from each other an amount equal to the interference fit. As a result, interference fits on the model cause a stress distribution before any of the operating loading conditions are applied. In this analysis, only interference fits were used for the gap elements.

The radial interference fit at each of the pilots was set by specifying a 0.0254-mm (0.001-in.) interference in the radial direction gap elements. The preload of the tie bolt was set by specifying an interference fit in all of the

axial gap elements. The desired tie bolt preload was chosen to be 47 148 N (10 600 lb); for the given bolt size, this load results in a bolt elongation of approximately 0.508 mm (0.020 in.). Since there are five axial contact surfaces, each of the gap elements at these surfaces were given an interference fit of 0.1016 mm (0.004 in.). This method seems to represent the effects of the preloaded tie bolt quite accurately.

As boundary conditions, all of the nodes along the axis of rotation were constrained against radial motion. Also, the node points located at the connecting bolt diameter, between the front shaft and the first disk, were tied together in the axial direction. This simulates a rigid bolted connection.

The stress-compatibility analysis of this system requires a nonlinear solution, therefore the system equations must be solved incrementally by the MARC finite element program. The governing equations are expressed in an incremental form as

$$K \, du = df$$

where du and df are incremental displacement and force vectors respectively and K is the stiffness matrix. The model was loaded with nine successive equal load increments. After the ninth load increment was applied, the total load on the model was equivalent to the actual loads at 47 500 rpm. The loading increments were specified within the input file such that the finite element program applies them automatically in one computer run. The element temperatures were applied to the model before the first load increment by reading them off of the computer tape created in the heat transfer analysis. One ninth of the centrifugal load and blade loads was then applied at each of the following nine load increments. The blade loads were applied as distributed nodal point loads.

If a gap develops during one of the load increments, the stiffness matrix changes and must be recalculated. The MARC program uses the full Newton-Raphson method as the solution procedure to determine the new stiffness matrix. Within each load increment, the program performs iterations, recalculating and refactorizing the stiffness matrix until the convergence criterion is met. Convergence is met when the ratio of the maximum residual force to maximum reaction force is less than a given tolerance.

The complete analysis required only two computer runs: one for the heat transfer analysis and the other for the stress-compatibility analysis. The program calculated the nodal displacements and gap element conditions after every load increment. The element stresses were calculated after the ninth (final) increment only, although they could have been asked for at any or all of the increments.

RESULTS AND DISCUSSION

The flexibility analysis method utilized the FEATS finite element computer program in order to obtain certain values within the set of compatibility equations and also to perform the final stress analysis of the rotor components. This effort required a total of 31 separate finite element computer runs. A simultaneous solution of the matrix of compatibility equations had to be made three times to solve for the final unknown forces.

The improved analysis method, or gap element method, required only one finite element computer solution to determine the operating stresses and to determine the compatibility of all contacting surfaces for the compressor rotor. There were no compatibility equations to solve. A steady-state heat transfer analysis was done prior to the stress analysis in order to determine the element temperatures that were used as the thermal loading conditions. This heat transfer analysis did not require much time or effort since the same finite element mesh was used as in the stress-compatibility analysis.

In both analysis methods, during operating conditions, the forces P_2 , P_4 , P_6 , and P_8 were all found to be equal to zero, which indicates that there are no moment forces between components. The pilot surfaces were all determined to be closed since the forces P_1 , P_3 , P_5 , P_7 , and P_9 all had positive values. Also, the tie bolt was tight since P_8 had a positive value. The forces resulting from each analysis method are shown in table II. The values given for these forces are integrated around the circumference of the pilot contact surface. The tie bolt load, P_8 , decreased from 47 148 N (10 600 lb) to approximately 33 800 N (7600 lb) during operation. This was expected since the Poisson's ratio effect slightly reduced the axial dimension of the assembly of components. The forces determined by the flexibility method compare quite well to those determined by the improved method with the largest discrepancy seen in the value for P_1 . One explanation for the differences may be that the improved method used an eight-noded element, which is much more accurate than the four-noded element that was used in the other method. Also, there are differences in the solution algorithms of the two finite element codes that were used.

Contour plots of the radial and tangential stress distribution on the components are shown in figures 6 to 11 for the flexibility method and in figures 12 to 17 for the improved method. The stress contours resulting from each analysis method compare very well to each other. The effects of the radial pilot loads can be seen by noticing that the radial stress is compressive (negative) at the pilot contact surfaces. Also, from examination of the elemental stress values, it was found that the radial stress is continuous across the pilot interfaces at the point of contact, which is a required boundary condition (ref. 9). Generally, the peak tangential stress values on the disks are higher using the improved method. This can be attributed to the use of the eight-noded elements, which give better results in areas that have high stress gradients.

CONCLUDING REMARKS

The stress-compatibility results that were obtained by using the improved analysis method agree very closely with those that were obtained by using the flexibility analysis method. In both cases, the design of the compressor rotor is satisfactory for operation within the stated operating conditions.

The disadvantage of the flexibility analysis method is that it is more time consuming and tedious than the improved analysis method. Many finite element solutions had to be performed to determine data that was needed in the compatibility equations. This analysis method, being so tedious, is usually only performed at the maximum operating speed. Therefore, information such as displacements or pilot movement trends cannot be determined at lower speeds unless another analysis is performed. If the analysis determines that any or

all of the pilot contacts have opened during compressor operation, then the pilots have to be redesigned, possibly by reversing their orientation. This requires the formulation of new finite element models representing the modified components, and the complete analysis has to be performed again. In some cases, this cycle had to be completed four or five times before a satisfactory design was discovered.

In the case of the improved analysis method, redesigns are accomplished with relative ease, requiring only minor modification of the finite element model and a solution by the MARC program. Another advantage is that the force at each gap element can be output at the end of each load increment. Therefore, as the compressor rotor speed increases, the engineer can determine if the pilot contact surfaces are tending to tighten, which is a desirable condition. The flexibility analysis method only reveals the contact forces at the speed that the analysis was performed.

Given the ease, timeliness, and reliability of the improved analysis method, it is a preferred alternative when analyzing multicomponent rotating systems.

REFERENCES

1. Rao, M.N.B.; and Kumaran, K.S.S.: Stress Analysis of a Compressor Assembly Subjected to Mechanical and Thermal Loadings. 2nd Seminar on the Role of Computers in Structural Analysis, Design and Optimization, National Aeronautical Laboratory, Bangalore, India, 1974, pp. EPT-66 to EPT-105.
2. Reddy, J.N.: Energy and Variational Methods in Applied Mechanics. John Wiley & Sons, 1974.
3. Boresi, A.P., et al.: Advanced Mechanics of Materials. Third ed., John Wiley & Sons, 1978.
4. Saada, A.S.: Elasticity Theory and Applications. Robert E. Krieger Publishing Co., 1983.
5. Martin, H.C.: Introduction to Matrix Methods of Structural Analysis. McGraw-Hill, 1966.
6. Gere, J.M.; and Weaver, W.: Analysis of Framed Structures. Van Nostrand Co., 1965.
7. Swanson, J.A.: FEATS - A Computer Program for the Finite Element Thermal Stress Analysis of Plane or Axisymmetric Solids. WANL-TME-1888, Westinghouse Astronuclear Laboratory, 1968.
8. MARC General Purpose Finite Element Program, User Manual, Vols. A-D. MARC Analysis Research Corporation, 1983.
9. Timoshenko, S.: Strength of Materials. Third Ed., Van Nostrand, 1962.
10. Aerospace Structural Metals Handbook. Metals and Ceramics Information Center, Columbus, OH, 1987.

TABLE I. - MATERIAL PROPERTIES OF COMPRESSOR COMPONENTS^a

Alloy	Temperature		Modulus of elasticity		Poisson's ratio	Coefficient of thermal expansion	
	°C	°F	N/m	psi		m/m °C	in./in. °F
Ti-6Al-4V	-18 204	0 400	5.75x10 ⁹ 5.40x10 ⁹	16.5x10 ⁶ 15.5x10 ⁶	0.33 .33	8.82x10 ⁻⁶ 9.36x10 ⁻⁶	4.90x10 ⁻⁶ 5.20x10 ⁻⁶
AISI 4340 alloy steel	-18 204	0 400	10.45x10 ⁹ 9.41x10 ⁹	30.0x10 ⁶ 27.0x10 ⁶	0.30 .30	11.16x10 ⁻⁶ 13.32x10 ⁻⁶	6.20x10 ⁻⁶ 7.40x10 ⁻⁶
18-200 maraging steel	-18 204	0 400	9.13x10 ⁹ 9.13x10 ⁹	26.2x10 ⁶ 26.2x10 ⁶	0.264 .264	10.1x10 ⁻⁶ 10.1x10 ⁻⁶	5.60x10 ⁻⁶ 5.60x10 ⁻⁶

Alloy	Thermal conductivity		Mass density		
	W/m °C	Btu/sec-in. °F	kg/m ³	lb sec ² /in. ⁴	
Ti-6Al-4V	0.806 1.027	9.26x10 ⁻⁵ 1.18x10 ⁻⁴	4423 4423	4.14x10 ⁻⁴ 4.14x10 ⁻⁴	
AISI 4340 alloy steel	4.03 4.63	4.63x10 ⁻⁴ 5.32x10 ⁻⁴	7831 7831	7.33x10 ⁻⁴ 7.33x10 ⁻⁴	
18-200 maraging steel	4.35 4.35	5.00x10 ⁻⁴ 5.00x10 ⁻⁴	8002 8002	7.49x10 ⁻⁴ 7.49x10 ⁻⁴	

^aFrom reference 10. Properties are linearly interpolated between the temperature limits.

TABLE II. - PILOT SURFACE FORCES PREDICTED BY TWO ANALYSIS METHODS

Load	Force predicted by flexibility analysis method		Force predicted by improved analysis method	
	N	1b	N	1b
P ₁	43 928	9 876	29 392	6 608
P ₃	67 756	15 233	64 215	14 437
P ₅	77 360	17 392	76 857	17 279
P ₇	67 614	15 201	67 432	15 160
P ₉	149 221	33 548	139 520	31 367
P _B	34 107	7 668	33 813	7 602

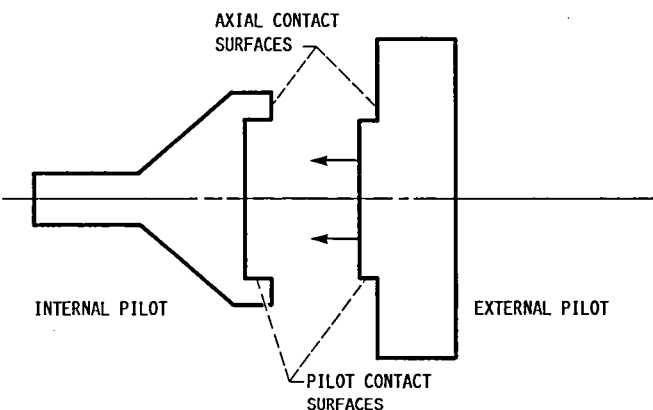


FIGURE 1. - TYPICAL PILOT DESIGN USED IN ROTATING MACHINERY.

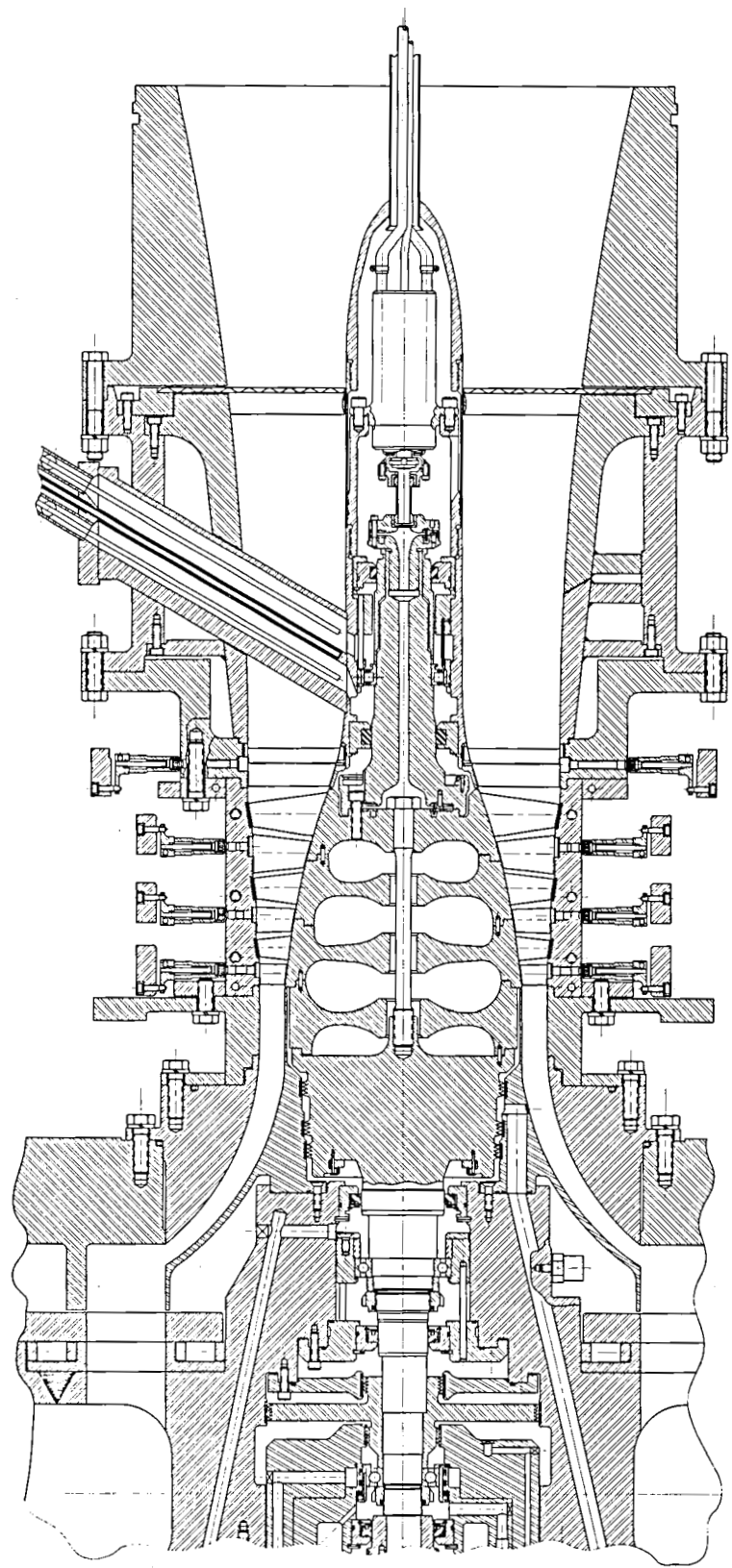


FIGURE 2. - THREE-STAGE AXIAL FLOW COMPRESSOR.

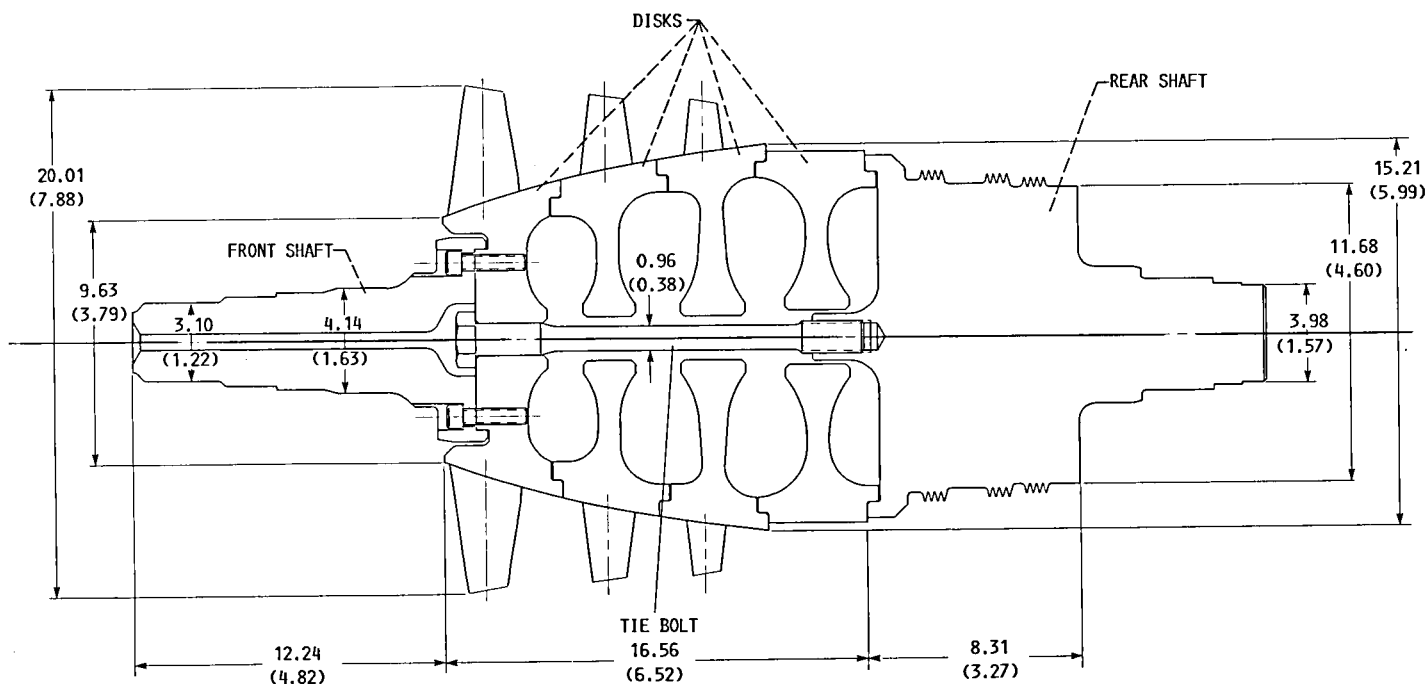


FIGURE 3. - COMPRESSOR ROTOR THAT WAS ANALYZED FOR STRESS AND COMPATIBILITY. ALL DIMENSIONS ARE GIVEN IN CENTIMETERS (INCHES).

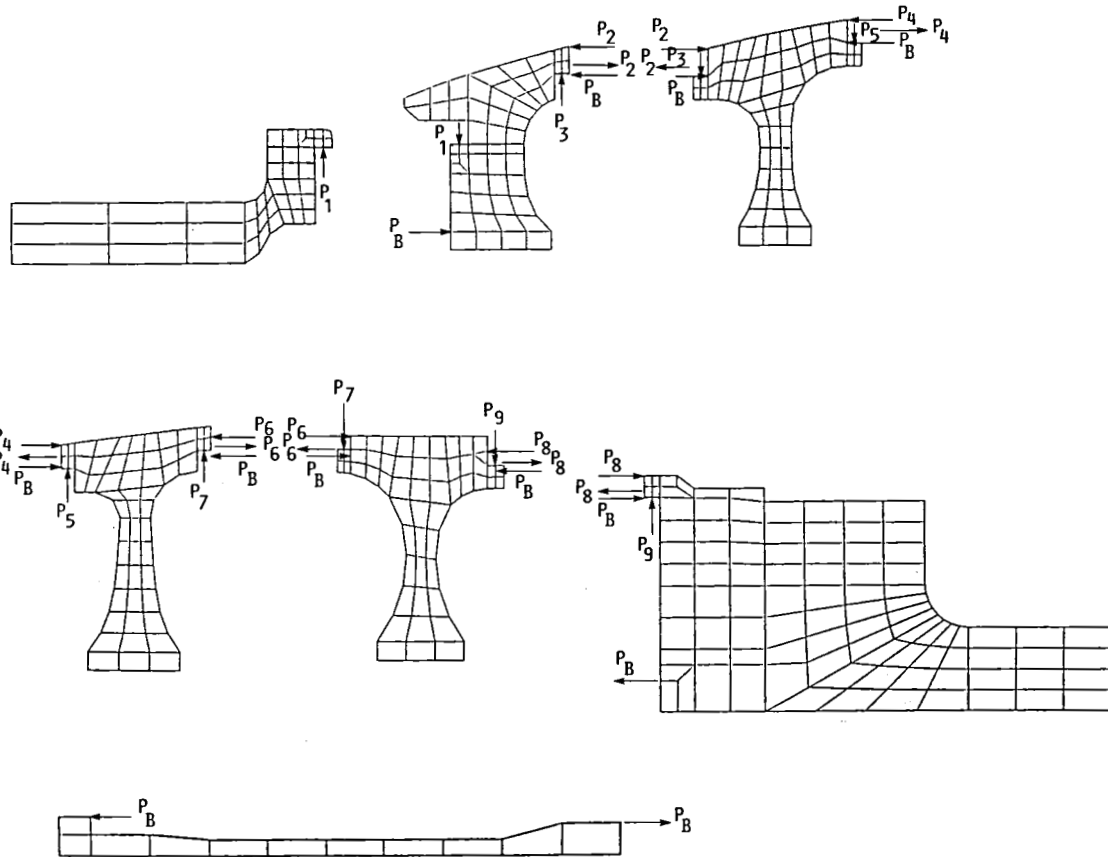


FIGURE 4. - FEATs FINITE ELEMENT MODELS WITH UNKNOWN INTERACTING FORCES.

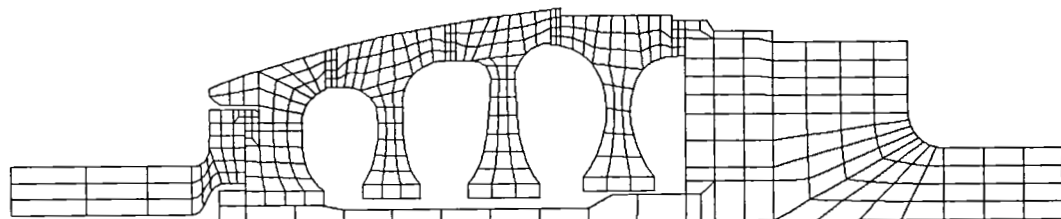


FIGURE 5. - MARC FINITE ELEMENT MODEL.

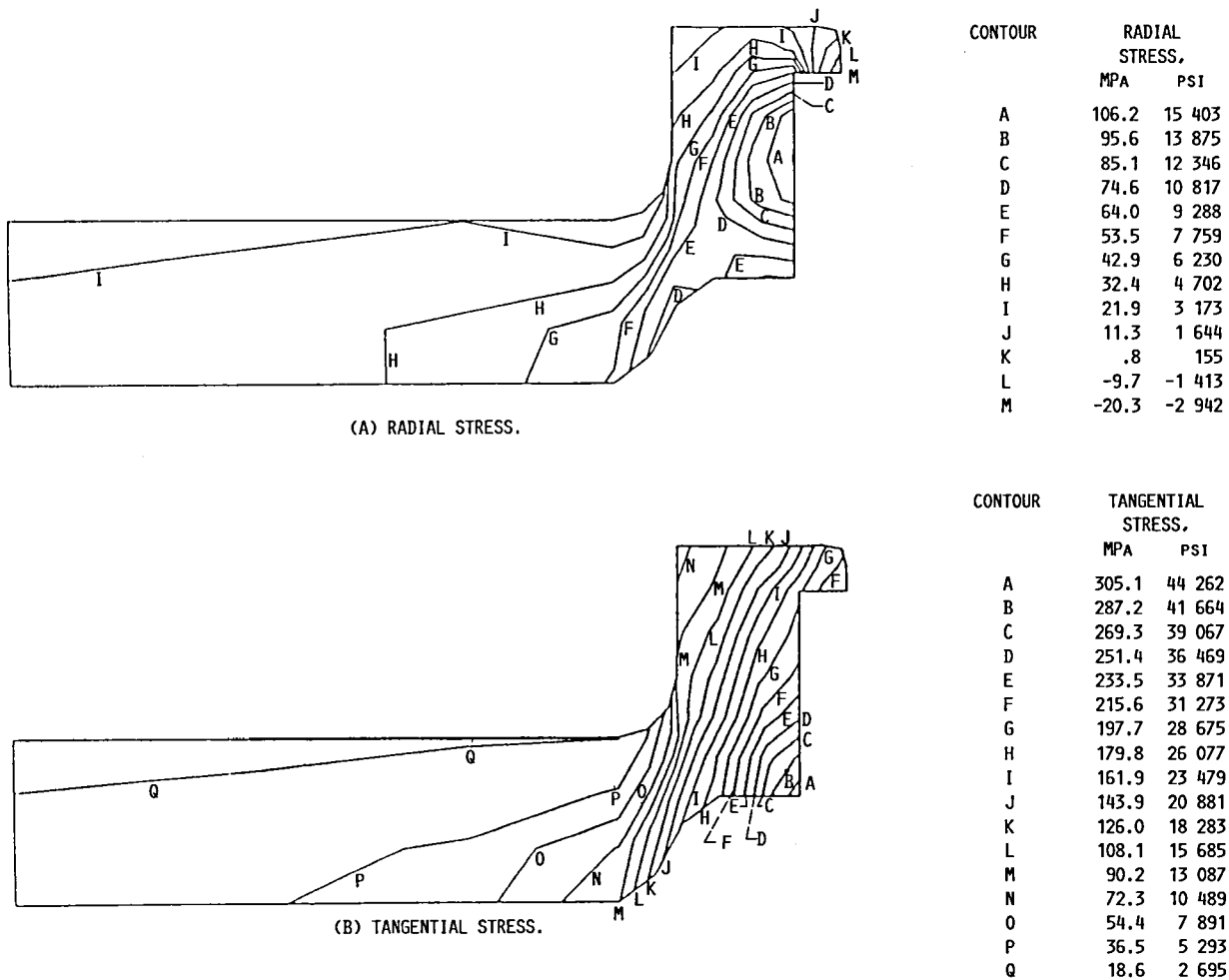
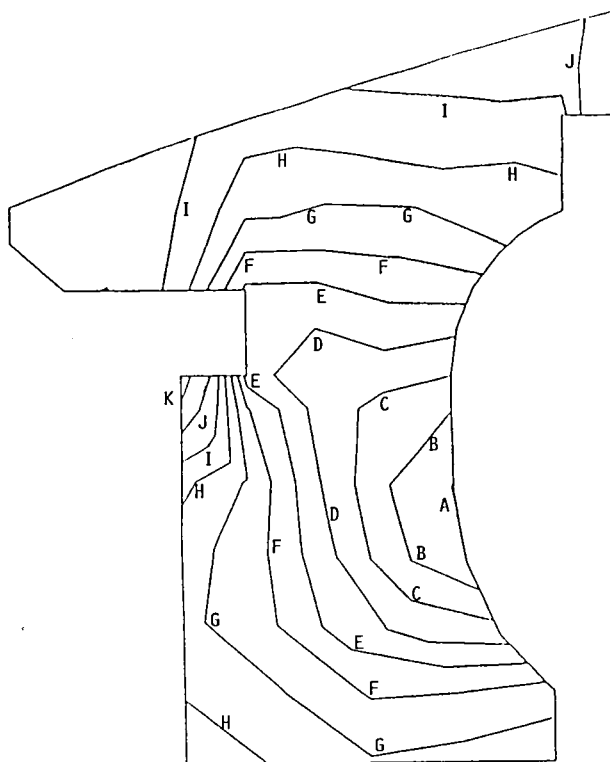
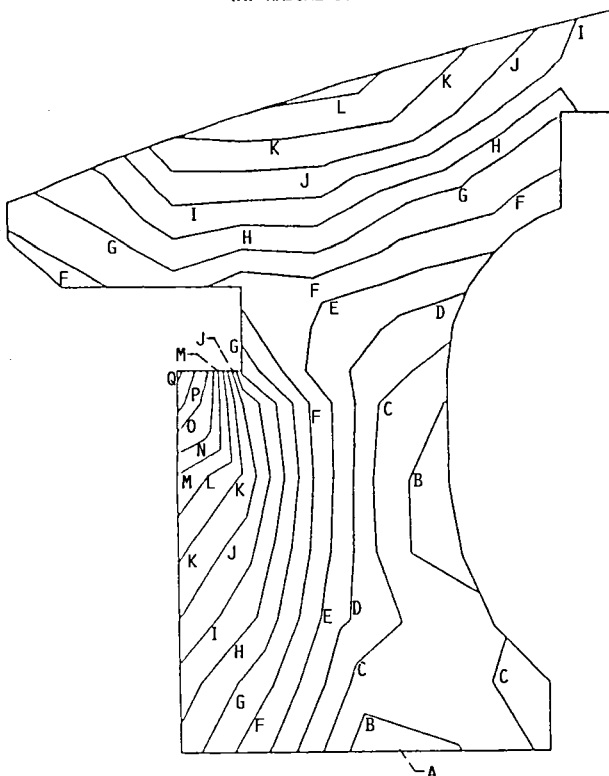


FIGURE 6. - STRESS CONTOURS FOR FRONT SHAFT PREDICTED BY FLEXIBILITY ANALYSIS METHOD.



(A) RADIAL STRESS.

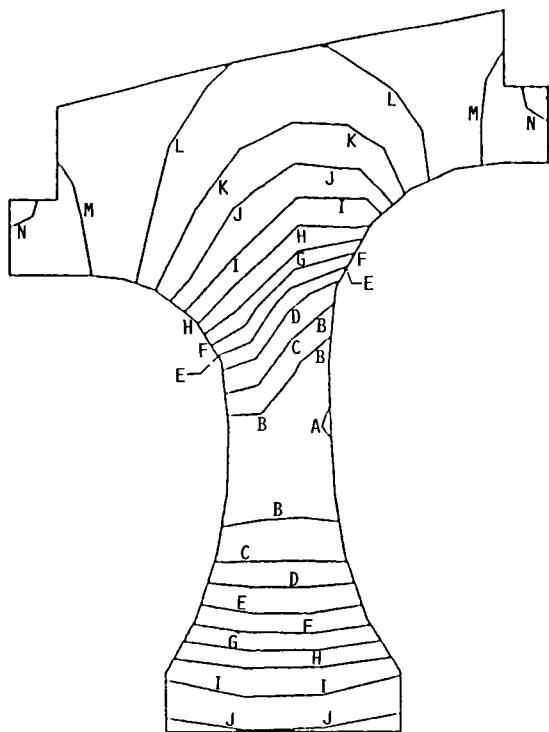
CONTOUR	RADIAL STRESS, MPa PSI	
A	264.7	38 399
B	235.8	34 199
C	206.8	29 999
D	177.8	25 799
E	148.9	21 600
F	120.0	17 400
G	91.0	13 199
H	62.0	9 000
I	33.1	4 799
J	4.1	600
K	-24.8	-3 600



(B) TANGENTIAL STRESS.

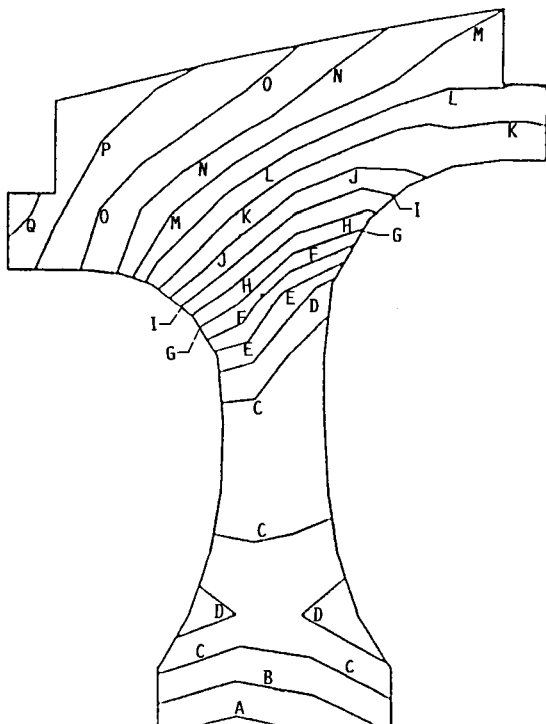
CONTOUR	TANGENTIAL STRESS, MPa PSI	
A	271.9	39 436
B	257.5	37 356
C	243.2	35 276
D	228.9	33 197
E	214.5	31 117
F	200.2	29 037
G	185.8	26 957
H	171.5	24 877
I	157.2	22 798
J	142.8	20 718
K	128.5	18 638
L	114.2	16 558
M	99.8	14 478
N	85.5	12 399
O	71.1	10 319
P	56.8	8 239
Q	42.4	6 159

FIGURE 7. - STRESS CONTOURS FOR FIRST DISK PREDICTED BY FLEXIBILITY ANALYSIS METHOD.



(A) RADIAL STRESS.

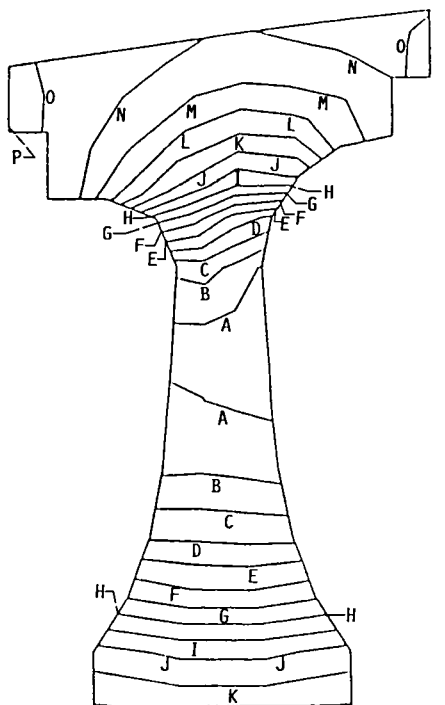
CONTOUR	RADIAL STRESS,	
	MPA	PSI
A	350.5	50 844
B	321.6	46 655
C	292.7	42 465
D	263.9	38 275
E	235.0	34 086
F	206.1	29 896
G	177.2	25 706
H	148.3	21 517
I	119.4	17 327
J	90.6	13 137
K	61.7	8 948
L	32.8	4 758
M	3.9	569
N	-24.9	-3 620



(B) TANGENTIAL STRESS.

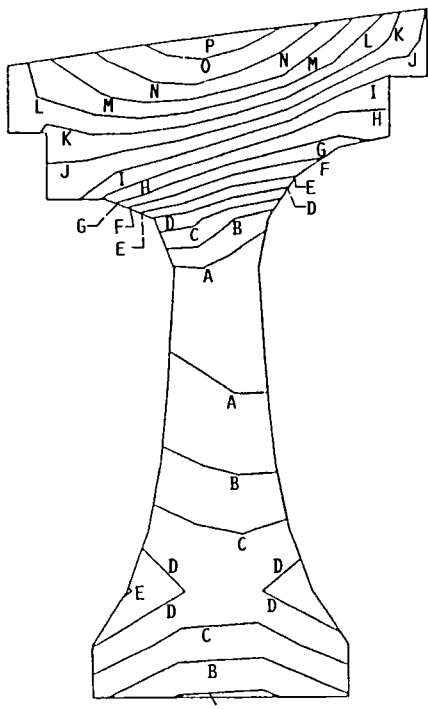
CONTOUR	TANGENTIAL STRESS,	
	MPA	PSI
A	361.2	52 395
B	347.3	50 373
C	333.3	48 351
D	319.4	46 329
E	305.4	44 307
F	291.5	42 285
G	277.6	40 263
H	263.6	38 241
I	249.7	36 219
J	235.7	34 197
K	221.8	32 175
L	207.9	30 153
M	193.9	28 131
N	180.0	26 109
O	166.0	24 087
P	152.1	22 065
Q	138.2	20 043

FIGURE 8. - STRESS CONTOURS FOR SECOND DISK PREDICTED BY FLEXIBILITY ANALYSIS METHOD.



(A) RADIAL STRESS.

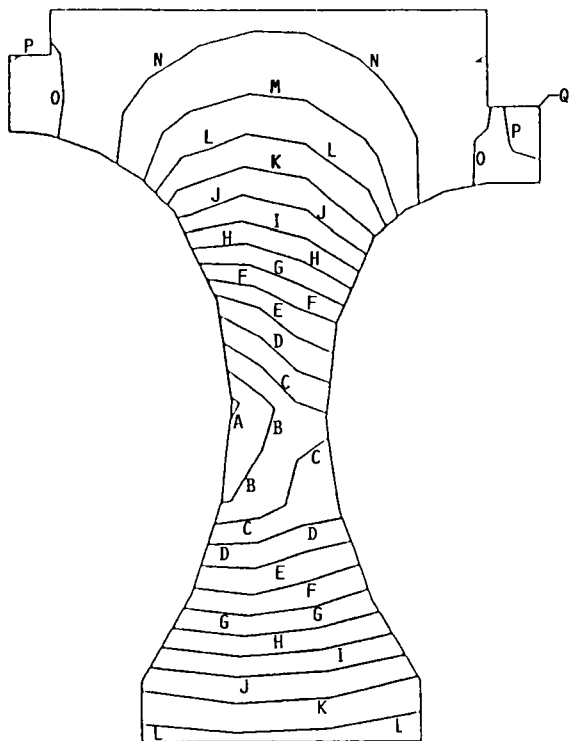
CONTOUR	RADIAL STRESS,	
	MPA	PSI
A	389.2	56 454
B	361.4	52 426
C	333.6	48 397
D	305.9	44 369
E	278.1	40 341
F	250.3	36 312
G	222.6	32 284
H	194.8	28 255
I	167.0	24 227
J	139.2	20 198
K	111.5	16 170
L	83.7	12 142
M	55.9	8 113
N	28.2	4 085
O	.4	56
P	-27.4	-3 971



(B) TANGENTIAL STRESS.

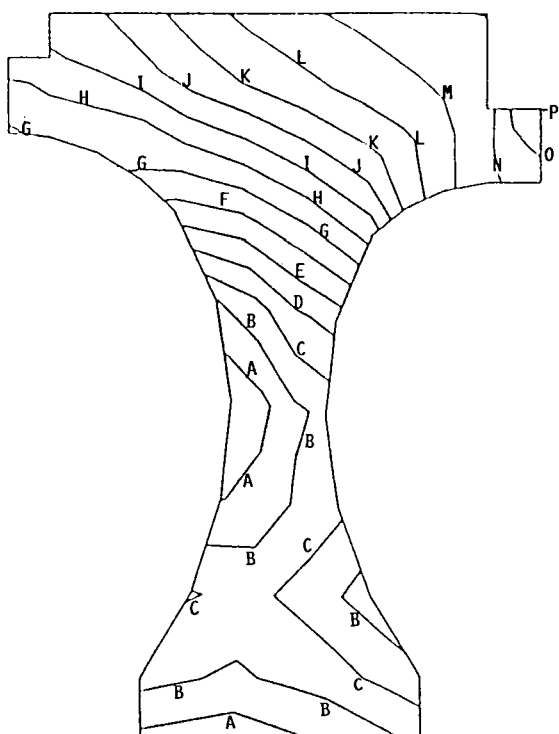
CONTOUR	TANGENTIAL STRESS,	
	MPA	PSI
A	389.0	56 425
B	375.0	54 400
C	361.1	52 375
D	347.1	50 350
E	333.1	48 325
F	319.2	46 300
G	305.2	44 275
H	291.3	42 250
I	277.3	40 225
J	263.3	38 200
K	249.4	36 175
L	235.4	34 150
M	221.5	32 125
N	207.5	30 100
O	193.5	28 075
P	179.6	26 050

FIGURE 9. - STRESS CONTOURS FOR THIRD DISK PREDICTED BY FLEXIBILITY ANALYSIS METHOD.



(A) RADIAL STRESS.

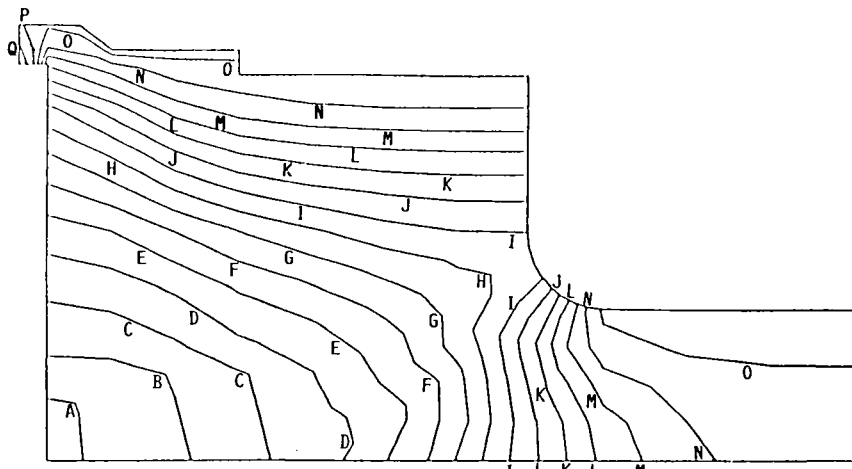
CONTOUR	RADIAL STRESS,	
	MPA	PSI
A	416.2	60 366
B	388.4	56 345
C	360.7	52 325
D	333.0	48 305
E	305.3	44 284
F	277.6	40 264
G	249.9	36 244
H	222.1	32 223
I	194.4	28 203
J	166.7	24 183
K	139.0	20 162
L	111.3	16 142
M	83.6	12 122
N	55.8	8 101
O	28.1	4 081
P	.4	61
Q	-27.3	-3 959



(B) TANGENTIAL STRESS.

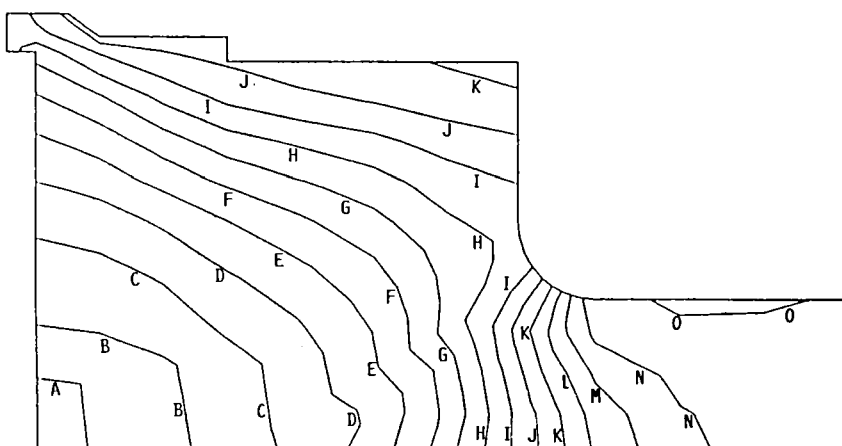
CONTOUR	TANGENTIAL STRESS,	
	MPA	PSI
A	383.1	55 571
B	365.6	53 037
C	348.2	50 504
D	330.7	47 970
E	313.2	45 437
F	295.8	42 903
G	278.3	40 369
H	260.8	37 836
I	243.4	35 302
J	225.9	32 768
K	208.4	30 235
L	191.0	27 701
M	173.5	25 168
N	156.0	22 634
O	138.6	20 100
P	121.1	17 567

FIGURE 10. - STRESS CONTOURS FOR FOURTH DISK PREDICED BY FLEXIBILITY ANALYSIS METHOD.



(A) RADIAL STRESS.

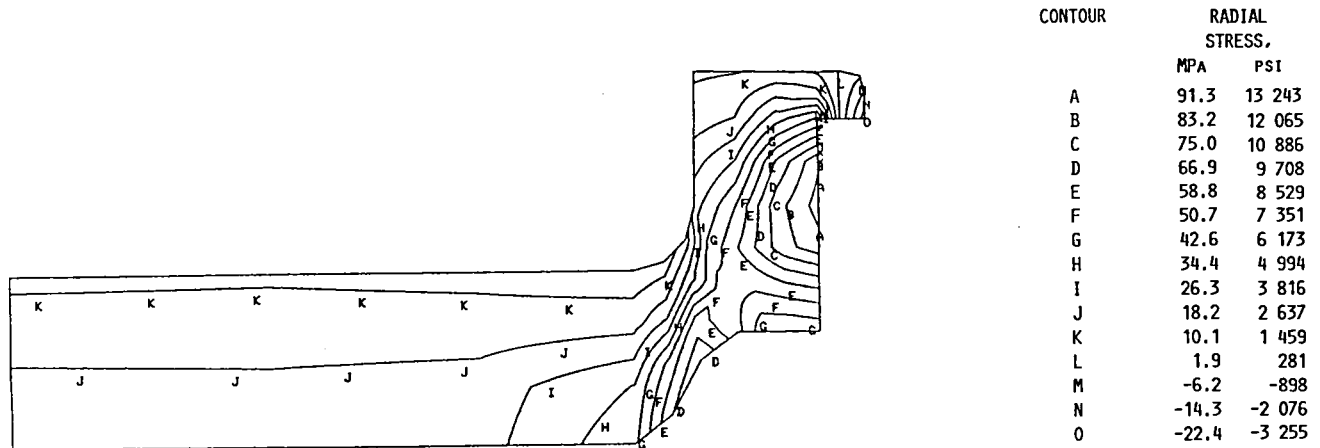
CONTOUR	RADIAL STRESS,	
	MPA	PSI
A	415.8	60 321
B	388.2	56 304
C	360.4	52 286
D	332.7	48 268
E	305.1	44 250
F	277.3	40 232
G	249.6	36 214
H	221.9	32 196
I	194.2	28 178
J	166.6	24 160
K	138.9	20 143
L	111.2	16 125
M	83.5	12 107
N	55.8	8 089
O	28.1	4 071
P	.4	53
Q	-27.3	-3 964



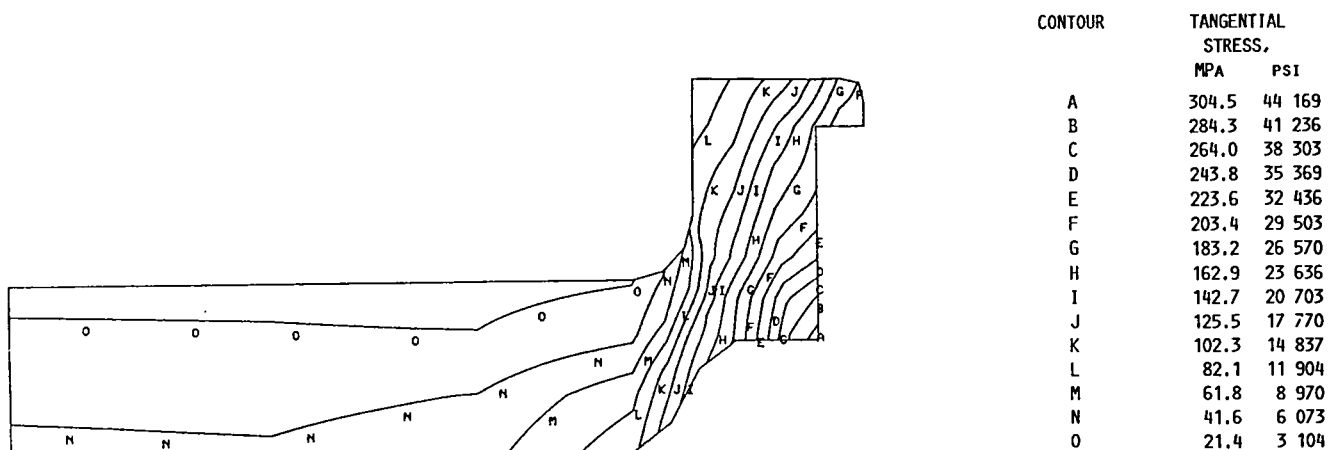
(B) TANGENTIAL STRESS.

CONTOUR	TANGENTIAL STRESS,	
	MPA	PSI
A	414.8	60 164
B	387.1	56 153
C	359.5	52 142
D	331.8	48 131
E	304.2	44 120
F	276.5	40 109
G	248.8	36 098
H	221.2	32 087
I	193.6	28 076
J	165.9	24 065
K	138.2	20 054
L	110.6	16 043
M	82.9	12 032
N	55.3	8 021
O	27.6	4 010

FIGURE 11. - STRESS CONTOURS FOR REAR SHAFT PREDICTED BY FLEXIBILITY ANALYSIS METHOD.

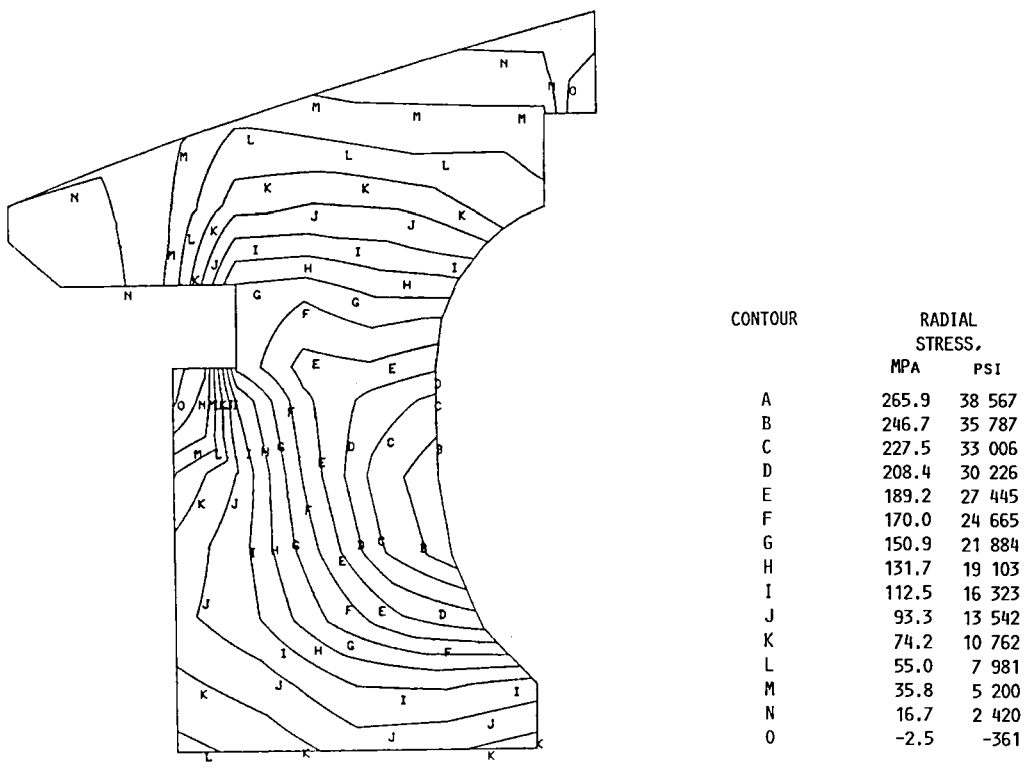


(A) RADIAL STRESS.

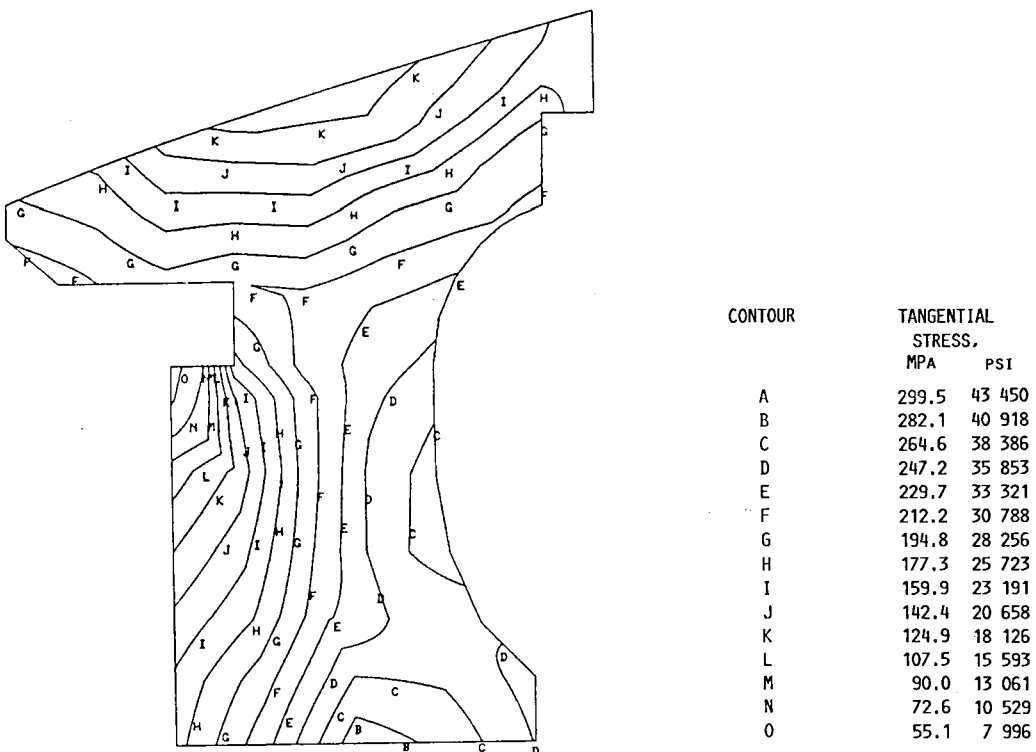


(B) TANGENTIAL STRESS.

FIGURE 12. - STRESS CONTOURS FOR FRONT SHAFT PREDICTED BY IMPROVED ANALYSIS METHOD.

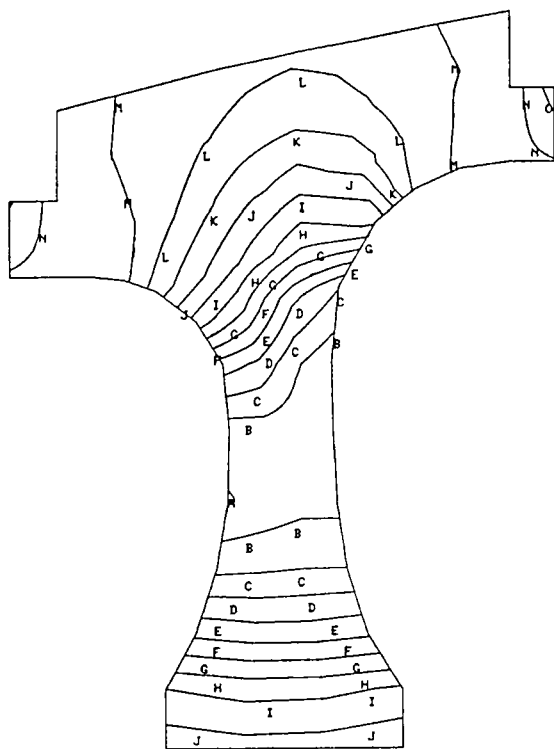


(A) RADIAL STRESS.



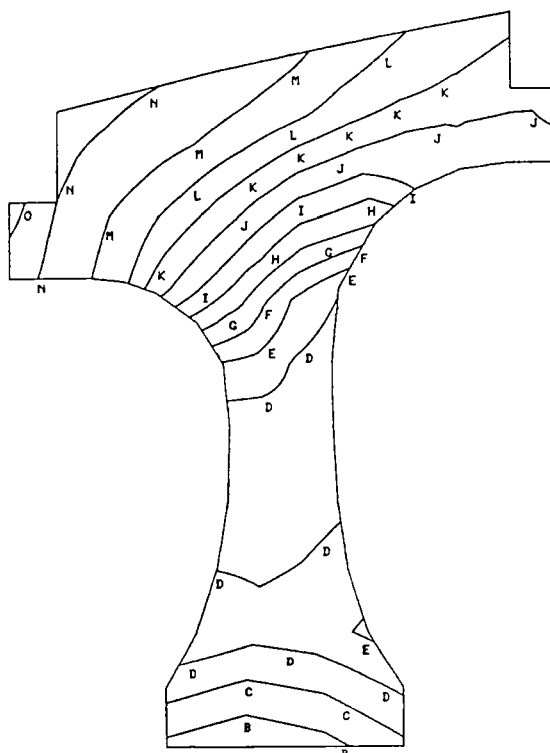
(B) TANGENTIAL STRESS.

FIGURE 13. - STRESS CONTOURS FOR FIRST DISK PREDICTED BY IMPROVED ANALYSIS METHOD.



(A) RADIAL STRESS.

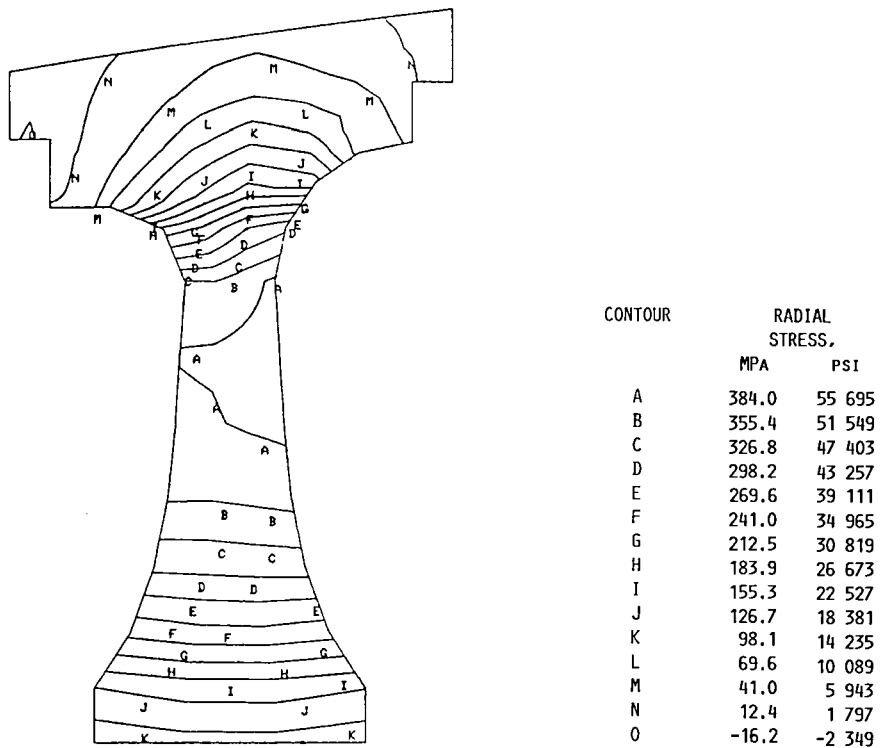
CONTOUR	RADIAL STRESS,	
	MPA	PSI
A	350.5	50 847
B	322.5	46 787
C	294.6	42 726
D	266.6	38 665
E	238.6	34 605
F	210.6	30 544
G	182.6	26 483
H	154.6	22 423
I	126.6	18 362
J	98.6	14 301
K	70.6	10 241
L	42.6	6 180
M	14.6	2 119
N	-13.4	-1 941
O	-41.4	-6 002



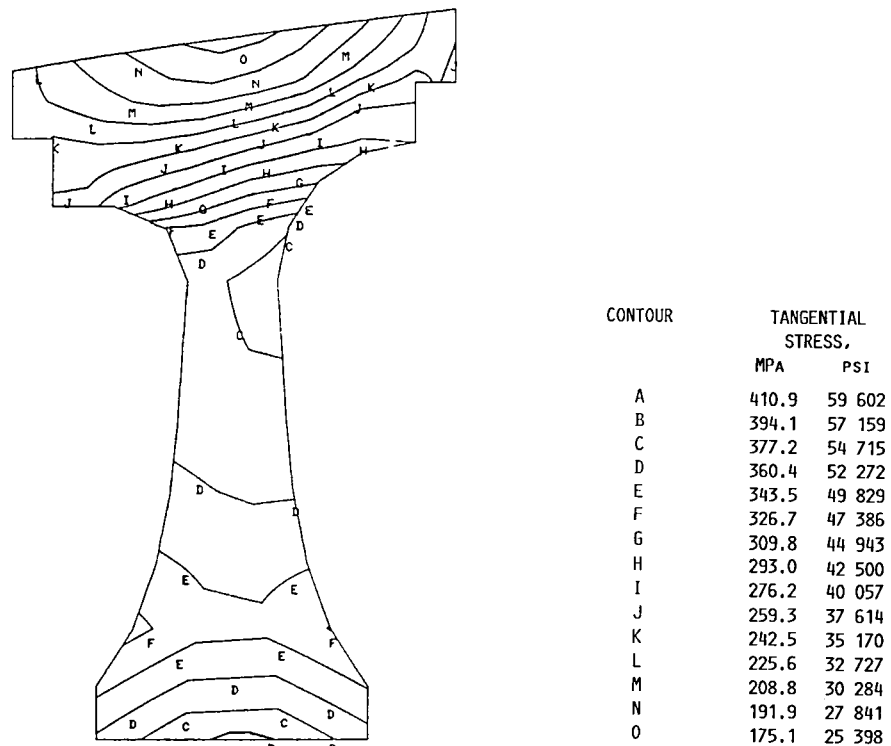
(B) TANGENTIAL STRESS.

CONTOUR	TANGENTIAL STRESS,	
	MPA	PSI
A	386.0	55 989
B	368.0	53 388
C	350.1	50 787
D	332.2	48 186
E	314.3	45 585
F	296.3	42 983
G	278.4	40 382
H	260.5	37 781
I	242.5	35 180
J	224.6	32 578
K	206.7	29 977
L	188.7	27 376
M	170.8	24 775
N	152.9	22 174
O	134.9	19 672

FIGURE 14. - STRESS CONTOURS FOR SECOND DISK PREDICTED BY IMPROVED ANALYSIS METHOD.

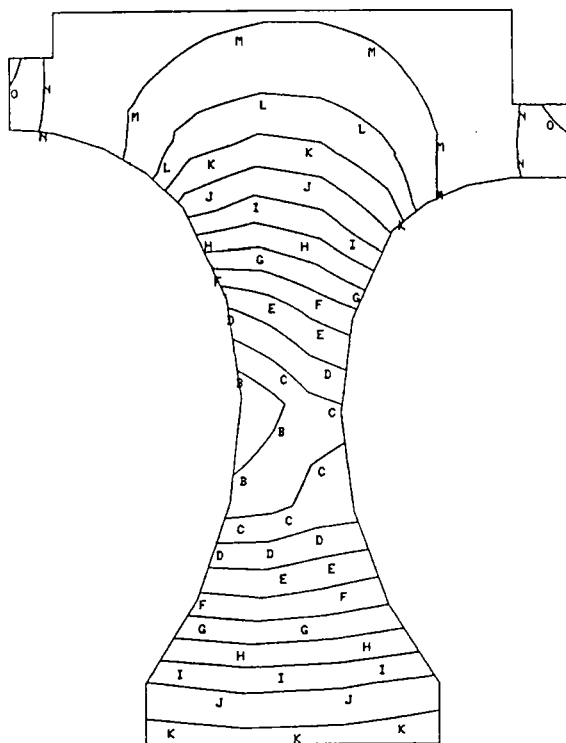


(A) RADIAL STRESS.



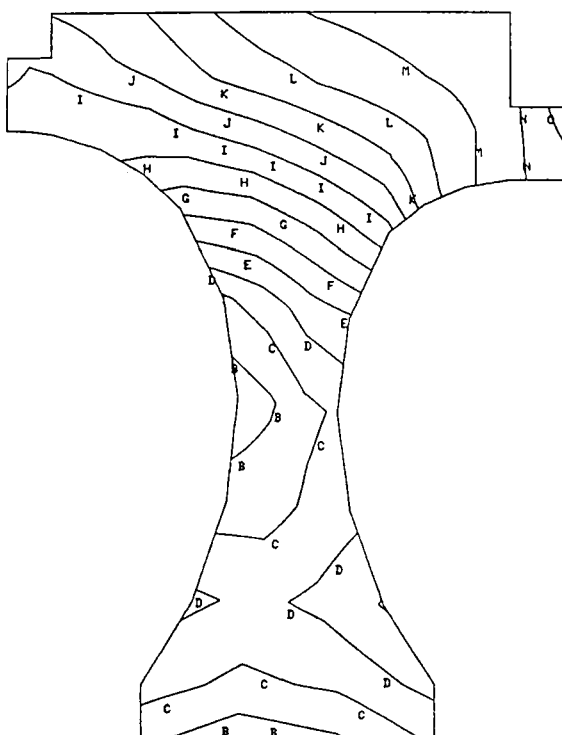
(B) TANGENTIAL STRESS.

FIGURE 15. - STRESS CONTOURS FOR THIRD DISK PREDICTED BY IMPROVED ANALYSIS METHOD.



(A) RADIAL STRESS.

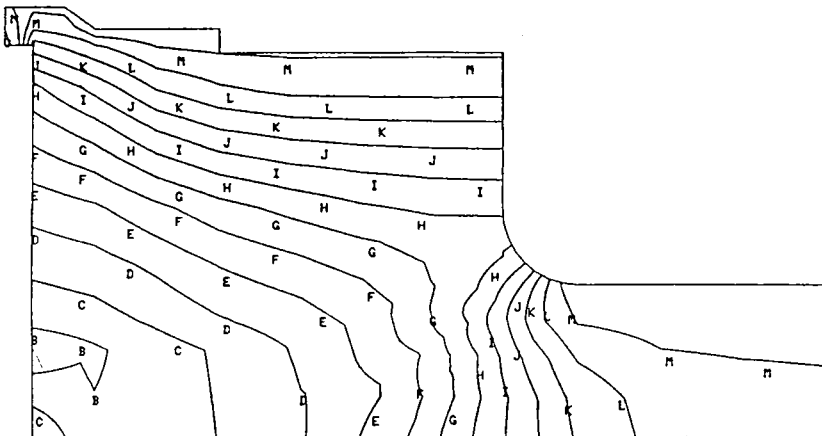
CONTOUR	RADIAL STRESS,	
	MPA	PSI
A	399.7	57 976
B	368.4	53 443
C	337.2	48 909
D	305.9	44 375
E	274.7	39 842
F	243.4	35 308
G	212.2	30 774
H	180.9	26 241
I	149.6	21 707
J	118.4	17 173
K	87.1	12 640
L	55.9	8 106
M	24.6	3 572
N	-6.6	-962
O	-37.9	-5 495



(B) TANGENTIAL STRESS.

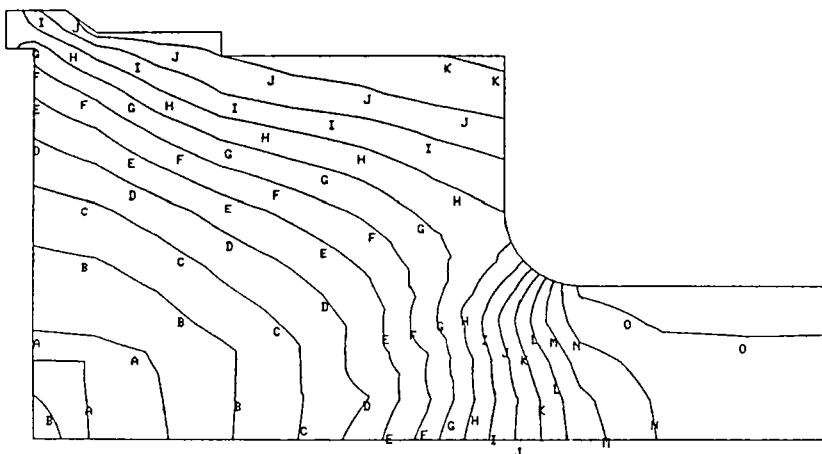
CONTOUR	TANGENTIAL STRESS,	
	MPA	PSI
A	389.2	56 463
B	370.5	53 741
C	351.7	51 020
D	333.0	48 299
E	314.2	45 578
F	295.4	42 856
G	276.7	40 135
H	257.9	37 414
I	259.8	34 692
J	220.4	31 971
K	201.6	29 250
L	182.9	26 529
M	164.1	23 807
N	145.4	21 086
O	126.6	18 365

FIGURE 16. - STRESS CONTOURS FOR FOURTH DISK PREDICTED BY IMPROVED ANALYSIS METHOD.



CONTOUR	RADIAL STRESS,	
	MPA	PSI
A	433.3	62 851
B	400.1	58 039
C	366.9	53 228
D	333.8	48 417
E	296.9	43 605
F	267.4	38 794
G	234.3	33 982
H	201.1	29 171
I	167.9	24 359
J	134.8	19 548
K	101.6	14 736
L	68.4	9 925
M	35.2	5 114
N	2.1	302
O	-31.1	-4 509

(A) RADIAL STRESS.



CONTOUR	TANGENTIAL STRESS,	
	MPA	PSI
A	389.4	56 494
B	364.1	52 807
C	338.6	49 120
D	313.2	45 434
E	287.8	41 747
F	262.4	38 060
G	237.0	34 373
H	211.5	30 686
I	186.1	26 999
J	160.7	23 312
K	135.3	19 625
L	190.9	15 938
M	84.4	12 251
N	59.0	8 564
O	33.6	4 877

(B) TANGENTIAL STRESS.

FIGURE 17. - STRESS CONTOURS FOR REAR SHAFT PREDICTED BY IMPROVED ANALYSIS METHOD.



National Aeronautics and
Space Administration

Report Documentation Page

1. Report No. NASA TM-100884	2. Government Accession No.	3. Recipient's Catalog No.	
4. Title and Subtitle Improved Method for Stress and Compatibility Analysis of Multicomponent Rotating Systems		5. Report Date June 1988	
		6. Performing Organization Code	
7. Author(s) Gerald A. Carek		8. Performing Organization Report No. E-4117	
		10. Work Unit No. None	
9. Performing Organization Name and Address National Aeronautics and Space Administration Lewis Research Center Cleveland, Ohio 44135-3191		11. Contract or Grant No.	
		13. Type of Report and Period Covered Technical Memorandum	
12. Sponsoring Agency Name and Address National Aeronautics and Space Administration Washington, D.C. 20546-0001		14. Sponsoring Agency Code	
15. Supplementary Notes			
16. Abstract <p>An improved method of analyzing multicomponent rotating assemblies for the determination of operating stresses and component compatibility has been developed. In this method, a single finite element model is developed which contains all of the separate components in the rotating assembly. This is made possible by using gap elements to simulate the contact surfaces between components. The MARC finite element computer program is then used to perform the analysis. This improved method is less time consuming and more reliable than the conventional method of analyzing such systems. Previously, a method called the flexibility method was used at the NASA Lewis Research Center for this task. It requires the individual analysis of components, derivation of compatibility equations, determination of certain coefficients for these equations, and an iterative solution procedure. This report presents results for two different stress-compatibility analyses of a six-component axial flow compressor rotor. The results for the flexibility analysis method are compared with those for the improved analysis method. It was found that the stresses predicted by each method compare quite well with each other. The predictions of the component compatibility, as well as the magnitude of the forces at the contact surfaces, also compare well for these two analysis procedures. It is therefore recommended that the improved analysis method be used to determine the stress-compatibility characteristics of multicomponent rotating systems.</p>			
17. Key Words (Suggested by Author(s)) Compatibility; Finite element; Pilot; MARC; Rotor		18. Distribution Statement Unclassified - Unlimited Subject Category 39	
19. Security Classif. (of this report) Unclassified	20. Security Classif. (of this page) Unclassified	21. No of pages 30	22. Price* A03

National Aeronautics and
Space Administration

Lewis Research Center
Cleveland, Ohio 44135

FOURTH CLASS MAIL

ADDRESS CORRECTION REQUESTED

Official Business
Penalty for Private Use \$300



Postage and Fees Paid
National Aeronautics &
Space Administration
NASA 451

NASA
